Materials Today Bio 27 (2024) 101128

Contents lists available at ScienceDirect

Materials Today Bio

journal homepage: www.journals.elsevier.com/materials-today-bio

Shear stress preconditioning and microbubble flow pattern modulate ultrasound-assisted plasma membrane permeabilization

Elahe Memari [a], Brandon Helfield [a,b,*]

[a] Department of Physics, Concordia University, Montreal, H4B 1R6, Canada
[b] Department of Biology, Concordia University, Montreal, H4B 1R6, Canada

ARTICLE INFO

Keywords:
Focused ultrasound
Endothelial secretome
Cytokine
Sonoporation
Targeted drug delivery

ABSTRACT

The recent and exciting success of anti-inflammatory therapies for ischemic heart disease (*e.g.* atherosclerosis) is hindered by the lack of site-specific and targeted therapeutic deposition. Microbubble-mediated focused ultrasound, which uses circulating, lipid-encapsulated intravascular microbubbles to locally enhance endothelial permeability, offers an exciting approach. Atherosclerotic plaques preferentially develop in regions with disturbed blood flow, and microbubble-endothelial cell membrane interactions under such flow conditions are not well understood. Here, using an acoustically-coupled microscopy system, endothelial cells were sonicated (1 MHz, 20 cycle bursts, 1 ms PRI, 4 s duration, 300 kPa peak-negative pressure) under perfusion with Definity™ bubbles to examine microbubble-mediated endothelial permeabilization under a range of physiological conditions. Endothelial preconditioning under prolonged shear influenced physiology and the secretome, inducing increased expression of pro-angiogenesis analytes, decreasing levels of pro-inflammatory ones, and increasing the susceptibility of ultrasound therapy. Ultrasound treatment efficiency was positively correlated with concentrations of pro-angiogenic cytokines (*e.g.* VEGF-A, EGF, FGF-2), and negatively correlated with pro-inflammatory chemokines (*e.g.* MCP-1, GCP-2, SDF-1). Furthermore, ultrasound therapy under non-reversing pulsatile flow (~4–8 dyne/cm^2, 0.5–1 Hz) increased permeabilization up to 2.4-fold compared to shear-matched laminar flow, yet treatment under reversing oscillatory flow resulted in more heterogeneous modulation. This study provides insight into the role of vascular physiology, including endothelial biology, into the design of a localized ultrasound drug delivery system for ischemic heart disease.

1. Introduction

Atherosclerosis stands as a chronic inflammatory disease, characterized by thickening of large vessels due to the accumulation of low-density lipids (LDL), *trans*-endothelial migration of immune cells into the arterial walls, and the development of fatty plaques [1]. As the plaque progresses, it can begin to erode or rupture, resulting in severe clinical consequences including myocardial infarction, peripheral artery disease, and ischemic stroke. Indeed, this condition serves as a fundamental basis for the majority of cardiovascular disease (CVD) and ranks among the leading causes of death worldwide [2]. Although the multifactorial nature of the disease (*e.g.* hypercholesterolaemia) is systemic, atherosclerotic plaques preferentially develop in regions with disturbed blood flow patterns [3]. The current standard of treatment for atherosclerosis includes systemic administration of cholesterol-lowering agents such as statins (HMG-CoA reductase inhibitors) and anti-platelet drugs, alongside surgical interventions for severe cases of the disease [4]. However, given the limited efficacy of current treatments and the inability to prevent the reoccurrence of the disease, there is an urgent need for finding novel strategies to target the underlying causes of atherosclerosis. To this end, there has been an influx of investigations into the use of pharmacological agents that target inflammation directly, and these have shown excellent pre-clinical results (*e.g.* Ref. [5]). Leveraging this success, recent clinical data has highlighted the direct benefit of targeting the inflammatory pathway on patient outcomes [6,7]. Perhaps the most successful of which is the CANTOS (Canakinumab Anti-Inflammatory Thrombosis Outcome Study) trial [8], in which the systemic delivery of the neutralizing IL-1β antibody canakinumab (50–150 mg) was shown to reduce the risk of a first major adverse cardiovascular event (MACE) by 15 % in patients with prior myocardial infarction, along with a dose-dependent reduction in IL6 (19–38 %) and C-reactive protein levels (26–41 %). Despite these

* Corresponding author. Department of Physics, Concordia University 7141 Sherbrooke St. W, H4B 1R6 Montreal, Quebec, Canada.
E-mail address: brandon.helfield@concordia.ca (B. Helfield).

https://doi.org/10.1016/j.mtbio.2024.101128
Received 5 April 2024; Received in revised form 31 May 2024; Accepted 13 June 2024
Available online 14 June 2024

exciting results, canakinumab was not approved by the FDA for this indication due to an increased level of fatal infections, suggesting the need for robust spatial targeting of the therapeutic antibody.

In designing an efficient drug delivery system for atherosclerosis, it is crucial to appreciate how complex blood flow patterns at the atherosclerotic prone regions influence endothelial permeability and susceptibility to treatment. Indeed, endothelial cells detect shear flow patterns via mechanosensors, including membrane receptor kinases, integrins, ion channels, intercellular junctions, and cytoskeleton components [9]. The regulation of endothelial gene expression via such mechanosensors in response to local shear stress is considered a major deterministic factor in atherosclerosis susceptibility [3]. Endothelial cells subjected to sustained laminar or unidirectional pulsatile flow correlate with transcription profiles considered protective against atherosclerosis (*e.g.* downregulation of pro-inflammatory genes). However, at the vascular regions with complex geometry such as vessel branch points, bifurcation and curved areas that result in uneven or disturbed flow, endothelial cells are exposed to low shear stress with high temporal gradients including oscillatory shear [10]. These more complex flow profiles are correlated with pro-inflammatory and atherogenic phenotypes, resulting in an increased endothelial cell turn over rate, endothelial permeability, and vascular bed impairment [11]. It is therefore of interest to consider the influence of shear stress preconditioning on endothelial cell permeability and integrity. In recent decades, various drug delivery methods have been explored for targeted deposition of therapeutic molecules within the context of CVD, including atherosclerosis. Of particular interest is the emergence of ultrasound-assisted therapy, as echocardiography already plays a key role in the diagnosis and management of patients with CVD. Contrast ultrasound, which employs ultrasound contrast agent microbubbles, is approved for use for left ventricle opacification in both adult and pediatric patients, and used in many off-label clinical cardiac applications (*e.g* myocardial perfusion, neovascularization imaging) [12]. Intravenously injected microbubbles are small (1–8 μm) gas-core microspheres, stabilized by a thin flexible shell composed typically of phospholipids, that remain intravascular due to their size. Exposure to diagnostic ultrasound results in their nonlinear vibration which enables the detection and separation of their echo from that of the surrounding tissue [13]. Beside diagnostic applications, microbubbles have shown tremendous therapeutic potential [14], the most clinically advanced application of which is the reversible opening of the blood-brain-barrier for targeted drug delivery [15–17]. Indeed, depending largely on microbubble physics and the surrounding tissue properties, oscillating ultrasound-stimulated microbubbles – which result in local, rapid fluid motion within the vicinity of the bubble itself - can exert targeted bioeffects via the application of shear and circumferential stress to neighboring vessels and tissues, ranging from reversible cell permeabilization [18,19], modulation of intracellular Ca^{2+} flux [20–22], enhanced blood flow perfusion [23,24], and modulation of inflammatory responses [25]. Given this context, here we aim to investigate the influence of flow pattern and magnitude on ultrasound-assisted endothelial cell permeabilization, including laminar, non-reversing pulsatile, and reversing oscillatory conditions. First, we examine the effect of shear preconditioning on the susceptibility of endothelial cells towards ultrasound-enhanced permeability, with a particular focus on the influence of shear-mediated cytokine and chemokine expression. Next, we investigate how microbubble fluid flow patterns during ultrasound treatment alters its efficiency, motivated by the intrinsic differences in flow profiles at different anatomical sites, including those in atherosclerotic prone regions.

2. Materials and methods

2.1. General cell culture

Human umbilical vein endothelial cells (HUVEC, C2519A; Lonza, Walkersville, MD, USA) were cultured in endothelial cell growth medium (EGM-2; CC3162, Lonza), and maintained at 37 °C with 5 % CO2 and 95 % air atmosphere. Independent of culture condition, endothelial cells were cultivated in collagen-iv coated μ-Slide I Luer type with a single channel (Ibidi, Gräfelfing, Germany) at a density of 120,000 cells/cm^2. The slides used in this study have a growth surface area of 2.5 $cm^{2,}$ with channel heights ranging from 0.4 to 0.8 mm. Based on the experiment, endothelial cells were cultured either statically or under flow conditions for two days.

2.2. Flow apparatus

For fluid flow-based experiments, the ibidi fluidic system, consisting of fluidic units, pump system and flow control software, was employed. For all experiments, the fluidic units were mounted with a yellow-green perfusion set (10 ml syringe reservoirs, filters, 1.6 mm silicon tubing) and connected to a pump system to generate the fluid flow – ranging from laminar, non-reversing pulsatile, and reversing oscillatory flow patterns (Fig. 1). The ibidi flow software was used to regulate the flow parameters and create the fluid flow profiles. The shear-flow was calculated using the flow control software, given by $\tau = \alpha\eta \bullet \Phi$, where τ is shear stress (dyne/cm^2), η is dynamical viscosity (dyne•s/cm^2), Φ is the flow rate of the perfused medium (ml/min), and α is a constant that is dependent on the chamber geometry.

Prior to cell cultivation under flow, a unidirectional flow was generated using the ibidi pump system for at least 30 min to remove any air bubbles in the perfused medium. To cultivate cells under flow, independent of the flow pattern, an augmented gradient of fluid flow was applied for 2 h to allow the cells to adapt to the flow condition and prevent cell detachment from the growth surface. While laminar flow needed only one fluidic unit, pulsatile flow requires two fluidic systems: primary and secondary units (see Fig. 1a). The primary unit was mounted with a perfusion set and was used to generate a laminar flow with a long switching time to provide a lasting circulation of fluid in the fluidic system. Additionally, the secondary unit without any perfusion set was used to generate pulsations by interrupting the laminar flow with a frequency of either 0.5 or 1 Hz. The flow control software creates pulsations by periodically changing the flow rate during the short switching time of the secondary unit but with a constant flow direction (non-reversing pulsatile flow). The third flow pattern investigated in this study was oscillatory flow, created using two fluidic systems with separate perfusion sets but interconnected air pressure tubing (reversing oscillatory flow). Similar to the pulsatile flow, the primary unit generated a laminar flow, whereas the secondary unit applied oscillations by reversing the flow direction alternatively with a frequency of either 0.5 or 1 Hz (1s or 0.5s switching time, respectively).

2.3. Experimental protocol

The ultrasound delivery platform has been reported previously [26]. Briefly, a customized acoustically coupled inverted microscope (Ti2-A, Nikon, Melville, New York, USA) was developed by fixing a compatible support and coupling cone for the ultrasound transducer (single-element 1 MHz, unfocused, diameter 2a = 12.7 mm; A303S- SU, Olympus, Waltham, MA, USA) on the microscopy platform. The transducer was fixed at a 45° angle to the normal and 27 mm distance from the cell monolayer surface. With this setup, the projected acoustic beamwidth at the microbubble-cell interface is approximately 3.5 mm. The transducer was driven by a signal generator (Tektronix, AFG31052 series, Chicago, USA) and amplified by a 150 W power amplifier (Amplifier research, Model: 150A 100B, Mississauga, USA).

2.4. Fluorescence markers

For real-time fluorescence imaging, cell nuclei were stained using Hoechst dye (Thermo Fisher) at a dilution of 1:500 v/v and maintained at 37 °C for 10 min, followed by washing with PBS (3x). To visualize cell

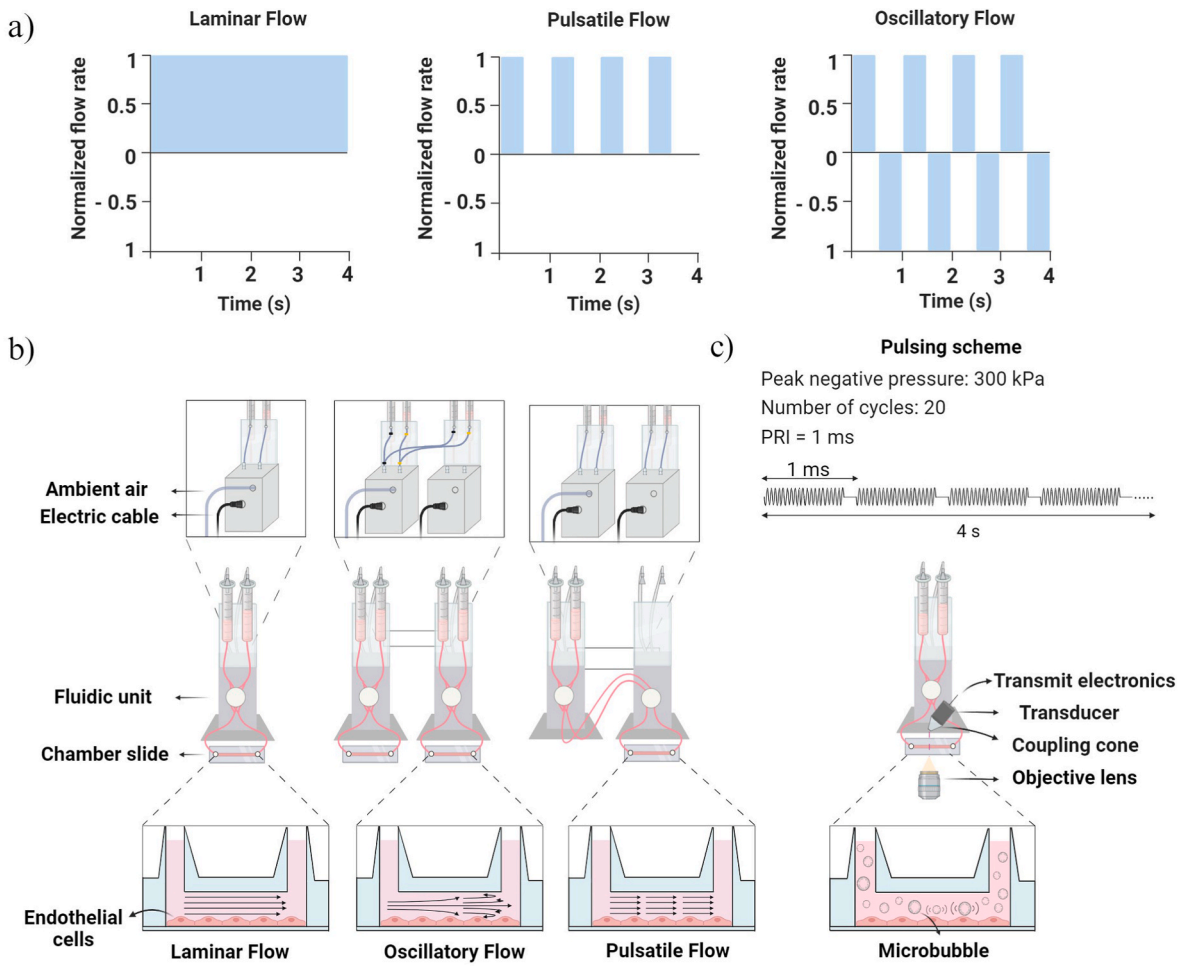

Fig. 1. Schematic overview of the experimental apparatus and flow conditions. a) Sample timing diagrams illustrative of the flow patterns used in this study, depicting laminar flow (left), non-reversing pulsatile flow (middle), and reversing oscillatory flow (right). Pulsatile and oscillatory flow frequencies ranged from 0.5 to 1 Hz (1–0.5 s switching time), and the ultrasound experiments were conducted for a fixed duration of 4 s. See specific experiments for details on shear magnitude/flow velocity, and the Methods text for the justification of their values in the context of healthy and atherosclerosis-prone regions. b) Overview of the tubing arrangements for the ibidi units required to achieve such flow patterns. c) Schematic view of the ultrasound pulsing scheme used throughout this work, as well as the acoustically-coupled microscopy system employed to examine microbubble-assisted endothelial permeability under flow.

permeabilization induced by ultrasound-stimulated microbubbles, propidium iodide (PI; 450 μM, P1304MP; Molecular Probes) was used as a real-time marker. This is a standard stain to differentiate permeabilized from non-permeabilized live cells since it is impermeable to cells with intact plasma membranes. Upon penetration into the cells, it binds to DNA, becoming fluorescent by shifting the fluorescence excitation/emission from 493/636 to 535/617 nm. Here, we employ it as a surrogate drug and real-time marker for ultrasound-assisted enhanced endothelial permeabilization, as has been done previously [27]. As it does not fluoresce within the bulk solution, real-time recording during treatment of time-dependent cellular permeability is possible due to the fact that the fluorescence intensity enhances only as it becomes intracellular.

2.5. Immunohistochemistry

To assess the effect of cell cultivation conditions on cell physiology, the endothelial cells were seeded in the 0.4 mm chamber slides either statically or under a pulsatile flow profile. Two days post-cultivation, cells were fixed using 2 % paraformaldehyde for 30 min. Subsequently, cells were permeabilized using 0.1 % Triton X100 for 10 min, followed by blocking the non-specific interactions with milk powder plus 5 % bovine serum albumin (BSA) for 45 min, washed with BSA (5x). Next, cells were incubated with mouse anti-CD31 (PECAM-1) monoclonal antibody for 1 h at room temperature, followed by washing (5x) with BSA to remove the unbound primary antibodies. We are interested in PECAM-1 due to its known role as a mediator in atherosclerosis [28,29]. Afterward, cells were incubated with Alexa Fluor 488-conjugated donkey anti-mouse IgG (A21202, Invitrogen) for 1 h, and washed (5x) with BSA. Actin filaments were counterstained with Alexa fluor 647-labeled phalloidin (A22287, Invitrogen) with a dilution of 1:400 v/v for 20 min and the unbound phalloidin was removed using washing (5x) with PBS. Cells were stained with either primary or secondary antibodies alone as negative controls. Cell nuclei were stained with DAPI with a dilution of 1:500 v/v. All the immunostaining steps were performed at room temperature. At least five random regions from each slide were imaged using a four-channel fluorescence inverted Nikon microscope with a 40× objective lens.

2.6. Shear stress preconditioning on ultrasound-assisted membrane permeabilization

To examine the effect of cell culture condition on cell susceptibility to sonication, endothelial cells were cultured in μ–Slides with a 0.8 mm channel height, either statically or under pulsatile flow for two days prior to the ultrasound treatment. For cultivation under pulsatile flow, cells were seeded statically for 2 h, followed by an augmented gradient of shear flow up to 8 or 16 dyne/cm^2 with a 1 Hz pulsatile frequency. For

the ultrasound treatment, cell-seeded slides were connected to a fluidic system, followed by perfusion of the chamber slides with a cocktail consisting of Definity™ microbubbles (1:500 dilution) and PI in culture media under pulsatile flow. Independent of culture conditions, cells were treated under the same two pulsatile flow regimens as they were cultured with: either at 8 or 16 dyne/cm^2 at a 1 Hz pulsatile frequency. After incubating the slide under flow for at least 30s to ensure a homogeneous distribution of microbubbles, each slide was sonicated (1 MHz frequency, 20 cycles, 1 ms pulse repetition frequency, 300 kPa peak-negative pressure) for a treatment duration of 4s, while the flow of microbubbles was maintained throughout the ultrasound treatment. Simultaneously, fluorescence microscopy recordings were obtained for 90s. The fluorescence microscopy recordings were started 8s before sonication to obtain information on the extent of baseline PI signal prior to sonication. Four non-overlapping locations from each sample were acquired (total growth area per slide of 250 mm^2), and the percentage of cells that were permeated under US and microbubble therapy was quantified using in-house software in MATLAB. The selection of these acoustic conditions was based on ensuring no cell detachment while exhibiting reliable measurable signal from the microscopy system over the range of flow rates employed in this study; following our previous work [26]. Further, the acoustic field in free space as well as the loss of signal due to the presence of the chamber slide (~5 % attenuation of signal) was measured using a hydrophone (Onda Corp., Sunnyvale, CA, USA, HGL-200); as previously reported [26]. Despite this, we do expect some proportion of reflected ultrasound within the chamber itself, resulting in the potential for an uneven acoustic field. Given that results and interpretations therein are relative (*i.e.* the independent variables are shear preconditioning, flow magnitudes, and flow patterns all under a fixed ultrasound condition and acoustic field), we do not foresee this as a confounding factor. All experiments were completed within 10 min after commencing flow with the diluted microbubble agent.

2.7. The effect of shear stress on endothelial cytokine expression profile

To assess the effect of pulsatile flow on cytokine release from endothelial cells, cells were seeded under the same pulsatile conditions as for the previous section (8 or 16 dyne/cm^2, 1 Hz). Simultaneously, cells with the same confluency were cultured statically as control (to mimic ischemic conditions). Two days post-cultivation, 100 μl of cell culture media was collected from each chamber slide, with two repeats for each condition. To examine the cytokine profile, a multiplex assay was used to analyze 96 human cytokines and growth factors (human immunology panel, Bio-Rad Laboratories, Hercules, CA). This multiplex assay functions via fluorescent detection of any array of color-coded beads conjugated to a specific capture antibody. The data was analyzed via a bead analyzer (Bio-Plex 200, Bio-Rad), which combines 2 lasers and high-throughput fluidics.

2.8. The influence of microbubble perfusion pattern on ultrasound-assisted permeabilization

To exclude the effect of cultivation conditions on the efficiency of US-mediated therapy, endothelial monolayers were cultured statically in chamber slides for two days before ultrasound delivery. First, the impact of pulsatile flow on microbubble-assisted endothelial cell perforation was assessed by connecting the slides to fluidic systems with either laminar or pulsatile flow (15–30 ml/min, 0.5–1 Hz). To further explore physiologically relevant flow conditions, a subset of the slides was connected to the secondary flow unit with an oscillatory flow profile; consisting of either a flow rate of 8 or 16 ml/min and an oscillation frequency of 0.5 or 1 Hz. In both pulsatile and oscillatory scenarios, four non-overlapping regions were sonicated with the same ultrasound conditions as given above, and real-time, simultaneous video recordings with two fluorescence channels for Hoechst and PI were recorded. The Hoechst channel was employed to determine the total number of cells within the field of view. To ascertain the overall count of permeabilized cells, in-house MATLAB software was written to quantify the extent to which cells were permeated over the 90s recording. As a fluid flow condition control, another subset of the slides was connected to the primary unit, co-perfused with microbubbles and PI under laminar flow and sonicated with the same ultrasound conditions.

2.9. Justification of shear stress magnitudes

In-vivo shear stress magnitudes have been reported to range from 10 to 70 dyne/cm^2 in healthy arteries, 1–6 dyne/cm^2 in veins, and ±4 dyne/cm^2 in atherosclerosis-prone arterial regions [10,30]. To examine the role of shear-stress preconditioning in the context of ischemic heart disease, the selection of shear magnitudes was chosen to represent flow conditions within ischemic (static; 0 dyne/cm^2), borderline (8 dyne/cm^2) and the lower range of healthy vasculature (16 dyne/cm^2). The flow velocities used to examine non-reversing pulsatile microbubble perfusion on statically cultured endothelial cells - stated here as flow rates instead of shear stress magnitudes due to the short perfusion time - do correspond to regions spanning recently re-perfused arterial vessels (~4–~8 dyne/cm^2). Finally, the dataset confirming the effects of reversing oscillatory shear to mimic disease-state disturbed flow are within the atherosclerosis-prone range (±2 and ± 4 dyne/cm^2 respectively [11,31]).

2.10. Statistical analysis

All data were analyzed using GraphPad prism and are presented as mean ± SEM. The fluorescence microscopy videos were analyzed using in-house software in MATLAB to quantify the percentage of cell perforation. The endothelial permeabilization datasets were repeated on at least five independent samples for each condition. The PECAM-1 mean fluorescence intensity was quantified using ImageJ from at least 8 random fields of view. Two-tailed, unpaired two-sample Student's t-tests were performed to determine the significance in comparison between treatment groups, using the Bonferroni multi-comparison correction when appropriate. Correlation coefficients and their associated statistics were calculated in MATLAB. For all datasets, a p-value of <0.05 was assumed to be statistically significant.

3. Results and discussion

Our previous work confirmed that the flow rate of laminar microbubble perfusion greatly influenced endothelial permeability and calcium intracellular signaling [26]. Here, we are examining the influence of shear-stress preconditioning, non-laminar microbubble perfusion, and their associated correlations as detailed below.

3.1. Shear stress preconditioning on ultrasound-assisted membrane permeabilization

Fig. 2a depicts a fluorescence microscopy example of how endothelial culturing condition influences cell physiological characteristics, such as morphology and cell-to-cell contact. As illustrated in Fig. 2a, statically cultured cells exhibited a heterogeneous orientation and morphology, characterized by large extracellular gaps due to the discontinuous distribution of intercellular junctional proteins. Conversely, cultured cells under pulsatile flow demonstrated a relatively aligned orientation in the direction of flow, more homogenous morphological features, and minimal extracellular gaps between cells. More specifically, these microscopy images highlight the effect of pulsatile flow cultivation on the expression of PECAM-1 (shown in green). PECAM-1 expression was highly heterogeneous in cells cultured statically, exhibiting regions of varying intensity. Under pulsatile flow, the expression of PECAM-1 became more pronounced as the shear-flow increased from 8 to 16 dyne/cm^2 at 1 Hz pulsatile frequency, as

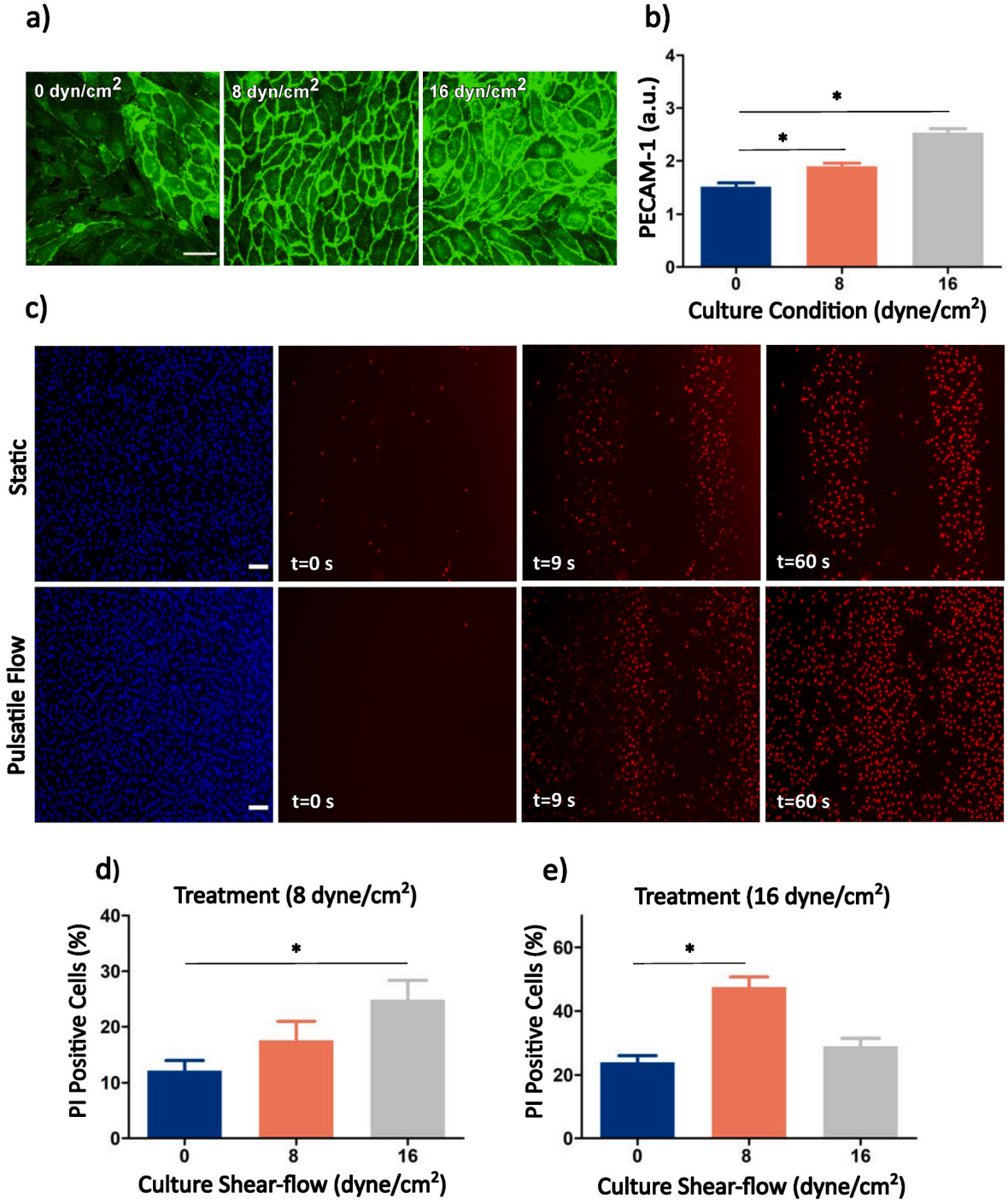

Fig. 2. Endothelial cell cultivation under pulsatile flow sensitizes cells to ultrasound-mediated cell permeabilization. a) Human endothelial cells were cultivated in chamber slides either statically or under pulsatile flow with shear stress magnitudes of either 8 or 16 dyne/cm^2 for two days. Immunofluorescence staining was performed for PECAM-1 (green). Fluorescence microscopy images demonstrate that cell cultivation under pulsatile flow leads to a more uniform cellular morphology, organized cell-to-cell contact, and reduced extracellular gaps between endothelial cells, as compared to statically cultured cells. Scale bar is 50 μm. b) Quantification of PECAM-1 expression illustrates a direct correlation between pulsatile shear flow and PECAM-1 expression. c) A representative example of time-lapse microscopy images from endothelial cells that were cultured either statically (top panel) or under pulsatile flow (bottom panel) during ultrasound treatment. Flow condition during ultrasound treatment remained constant within different subgroups. Nuclei were stained with Hoechst (blue) and the surrogate macromolecule (red) was used to indicate cell membrane permeabilization. d) Endothelial cells with microbubbles perfusing via a pulsatile flow of 8 dyne/cm^2 or e) 16 dyne/cm^2 exhibited an increased susceptibility to ultrasound-mediated cell permeabilization versus statically cultured cells (noted here as a culture shear-flow of 0 dyne/cm^2). The magnitude of this effect increased with variations in shear flow during cultivation and microbubble perfusion velocity. Asterisks denote statistical significance.

quantified in Fig. 2b ranging from 1.8 to 2.5-fold increase under shear-flow than static culturing ($p < 0.01$). Note here that the static culturing condition is denoted as 0 dyne/cm^2. Fig. 2 also shows how cultivation condition affects human endothelial cell sensitivity to ultrasound-mediated cell perforation. Here, we are examining the effect of endothelial culture preconditioning (static and pulsatile flow at either 8 or 16 dyne/cm^2 with 1 Hz pulsatile frequency) on the resulting endothelial susceptibility to ultrasound and microbubble treatment given the same acoustic stimulus. We investigated two different flow treatment regimes, with microbubbles circulating over the endothelial monolayer under pulsatile flow of 8 or 16 dyne/cm^2 to match the culturing conditions. Fig. 2c depicts a representative example of the time-lapse microscopy data of preconditioned endothelial monolayers (static [top] or under a pulsatile flow of 8 dyne/cm^2 [bottom]) undergoing microbubble therapy under the same treatment conditions, where the red denotes enhanced permeability as reported by intracellular PI entry. The first frame from each condition shows a Hoechst staining of the cell nucleus, which was used to quantify the number of cells in the field of view. Fig. 2d&e summarize our findings. With microbubbles perfusing the endothelial monolayers under a pulsatile flow pattern of 8 dyne/cm^2, those that were preconditioned under shear-flows of 8 or 16 dyne/cm^2 exhibited an augmented enhancement of ultrasound-assisted membrane permeability by 1.44 and 2.04-fold ($p < 0.005$) in comparison to those statically cultured, exhibiting an approximately linear trend (Fig. 2d). Further, those subjected to microbubble treatment under a pulsatile flow rate of 16 dyne/cm^2 similarly exhibited an increased sensitization to permeabilization based on shear-stress preconditioning, increasing by 1.98 ($p < 0.001$) with 8 dyne/cm^2 and 1.21-fold with 16 dyne/cm^2

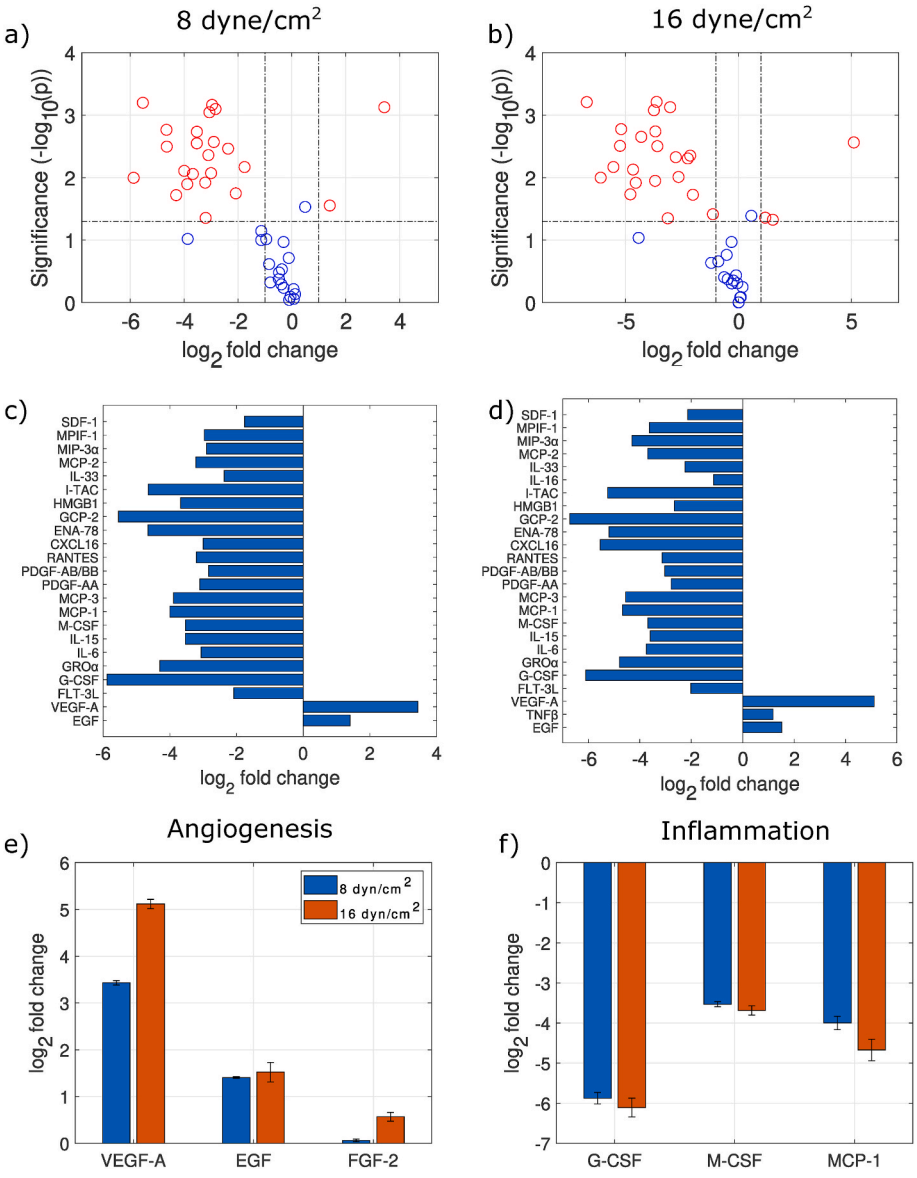

Fig. 3. Prolonged pulsatile shear-flow modulates human endothelial cell secretome. a,b) Volcano plots illustrating modulation of cytokine expression when exposed to 8 dyne/cm^2 or 16 dyne/cm^2 in comparison to statically cultured cells. Every analyte examined is represented with a circle – the ones shown in red demonstrate at least a 2-fold change and are statistically significant (dotted lines represent 2x increase [$log_2 = 1$] or 2x decrease [$log_2 = -1$], and the vertical line represents the line above which $p < 0.05$), whereas the blue dots represent analytes with a small change (less than 2-fold change) or no change, and are not statistically significant. c, d) Identification of those analytes with significant and large magnitude differential secretions upon endothelial cell cultivation (the red circles in the volcano plots). Select examples are shown for three cytokines with known involvement as e) pro-angiogenic and f) pro-inflammatory. Prolonged shear-stress preconditioning showed similar effects at both shear magnitudes: significantly downregulating many important factors of the endothelial secretome (*e.g.* pro-inflammatory) and upregulating those with pro-angiogenesis properties.

compared to static culturing, respectively. It is well established that endothelial cells exposed to prolonged fluid shear stress elongates their morphology to the direction of flow, in agreement with the results presented here. PECAM-1 is an established mediator of atherosclerosis and has been shown to influence the initiation and progression of atherosclerosis both negatively and positively, depending on the vascular site [32,33]. Further, PECAM-1 expression is correlated with increased vascular integrity [34] and changes in endothelial plasma membrane stiffness [35]. From a purely physical perspective, this change in cell morphology should increase the available cellular surface area – and thus probability for microbubble-cell interactions - for ultrasound-assisted permeabilization. In addition to this cell area-based argument, the plasma membrane biomechanics for a given endothelial cell are altered when pre-exposed to fluid shear, one major effect of which is to induce an increase in plasma membrane fluidity as compared to static controls [36,37]. Increased membrane fluidity is correlated with increased passive cellular permeability [38], and fluid flow shear preconditioning has been demonstrated to increase the baseline levels of human endothelial cell cellular permeability due to this average increased inter-phospholipid distance [39]. While not yet thoroughly investigated, there is some evidence that ultrasound-assisted cell permeabilization is facilitated when plasma membrane fluidity is increased [40], and thus consistent with the present findings. These results indicate that, overall, subjecting cells to a pulsatile flow pattern considerably enhances the endothelial cell sensitivity to the ultrasound-stimulated microbubbles.

3.2. The effect of shear stress on endothelial cytokine expression profile

To further investigate the relationship between shear preconditioning and susceptibility to ultrasound-mediated permeabilization, we assayed differential endothelial cell cytokine expression. Our findings indicate that cell cultivation under pulsatile flow at 8 and 16 dyne/cm^2 significantly altered the expression of 23 and 25 cytokines/growth factors, respectively, as compared to the statically cultured monolayers. Significance here is quantified as at least a 2-fold change that meets the threshold significance level of $p < 0.05$. Fig. 3a&b illustrate the volcano plots containing all the analytes with a concentration within the detectable range of the standard curve (8 and 16 dyne/cm^2, respectively). The analytes with out-of-range concentration, either below or above the standard curve, were excluded from the volcano plots. In these figures, each of the secreted molecules is represented by a circle. Those that exhibited at least a statistically significant 2-fold increase ($log_2 = 1$) or decrease ($log_2 = -1$) compared to static controls are illustrated in red along with nonsignificant and/or smaller changes denoted in blue. The analytes exhibiting large magnitude differential secretions are then depicted for each flow condition in Fig. 3c&d. It is interesting here to broadly categorize the cytokine functions within two major groups: angiogenesis and inflammation. Indeed, as expected, induction of prolonged flow significantly upregulated pro-angiogenesis factors, including vascular endothelial growth factor-A (VEGF-A), epidermal growth factor (EGF), and fibroblast growth factor-2 (FGF-2) - see Fig. 3e. Among these factors, the largest magnitude change is VEGF-A, which was upregulated by 10.7-fold and 34.5-fold (3.43 and 5.11-fold in log_2 units) under preconditioning of pulsatile flow of 8 and 16 dyne/cm^2 compared to static control, respectively. VEGF-A is a well-known modulator of vascular development and angiogenesis via its interaction with its endothelial receptor (mainly VEGFR2, although it also binds to VEGFR1). VEGF-A and other pro-angiogenic factors (*e.g.* FGF-2) have been identified as key endothelial survival signals involved in the maintenance of endothelial homeostasis and vascular integrity [41], the disruption of which helps mediate atherosclerosis [42]. Indeed, autocrine VEGF signaling – as is the case here – is known to play a critical role in maintaining endothelial cell viability [43]. It is well understood that VEGF-A, along with other pro-angiogenic markers, can disrupt endothelial cell-cell contacts (*e.g.* tight junctions, adherins), change endothelial cell morphology, and increase vascular leak [44]. Further, prolonged exposure of endothelial cells to VEGF-A can induce the formation of small pores (*i.e.* fenestrations) within the plasma membrane, allowing the uptake of small molecules [45,46]. It is therefore not particularly surprising that – under the influence of significantly increased concentrations of these pro-angiogenic cytokines, the endothelial cell membrane is more susceptible to permeabilization from mechanical perturbations (via microbubble vibrations) than otherwise, as it is already characterized by increased fluidity. Aside from these, Fig. 3 demonstrates a consistent downregulation of a broad range of pro-inflammatory cytokines, the majority of which are shared between the two shear conditions (*e.g.* G-CSF, M-CSF, MCP-1). It is important to note here that while some of these pro-inflammatory cytokines have been shown to exhibit time-dependent increases in secretion under flow for short periods of time (*e.g.* MCP-1 [47,48]), the data presented here is consistent with prolonged application of shear (>24 h). Indeed, the suppression of the myriad of pro-inflammatory secretions by long-term shear conditioning observed here is broadly consistent with many other works in which isolated cytokines were examined independently [49–51], as well as with the general downregulation of pro-inflammatory genes under chronic shear stress observed via microarray data [49,52,53].

While it is acknowledged here that the interaction between the complete endothelial secretome and how it influences the susceptibility of the plasma membrane to an external energy source like ultrasound is complex, it is perhaps still instructive to dissect the correlation between shear stress preconditioning and ultrasound-assisted enhanced permeability on an individual cytokine level. Specifically, Fig. 4 depicts nine noteworthy correlations that identify three global categories: angiogenesis, leukocyte chemotaxis, and lymphocyte chemotaxis, with correlation coefficients R ranging here from $0.82 \leq |R| \leq 0.99$. Note that while some display statistically significant correlations, many are highly trending towards significance. Firstly, it is interesting to note that ultrasound-assisted permeabilization is highly positively correlated with preconditioning from pro-angiogenic cytokines (VEGF-A, EGF, FGF-2) – Fig. 4a–c. In addition to these relations, ultrasound-assisted endothelial permeabilization was highly negatively correlated with pro-inflammation mediators, in particular those that both modulate leukocyte (*e.g.* MCP-1, GCP-2, MCP-3) and lymphocyte (*e.g.* I-TAC, SDF-1, CXCL16) chemotaxis, among more general inflammation markers (*e.g.* IL6, not shown). Indeed, many of these mediators can act in autocrine and play a role in endothelial migration and physiology (*e.g.* CXCL16 [54], MCP-1 [55]). It is of interest to note that the endothelial plasma membrane itself is a known mechano-sensor, and when placed under shear stress exhibits a marked reduction in its cholesterol content [56]. This has implications when considering lipid rafts – a potent platform for signal transduction – the disruption of which can hinder cytokine signaling and attenuate the cytokine response [57–59]. In fact, the majority of differentially secreted cytokine/chemokines were downregulated under flow (Fig. 3c&d) and thus correlate negatively with membrane fluidity and ultrasound-assisted membrane permeabilization (Fig. 4d–i).

3.3. Microbubble perfusion flow pattern and endothelial cell permeabilization

Irrespective of preconditioning, we next explored how the fluid pattern of the perfusing microbubbles during ultrasound treatment modulated the therapeutic result. Firstly, pulsatile perfusion was compared to flow rate-matched laminar perfusion (Fig. 5). Representative microscopy images (Fig. 5a) reveal qualitatively that pulsatile flow results in an increase of ultrasound-assisted membrane permeability, the effects of which are quantified at two flow rates of 15 and 30 ml/min in panels Fig. 5b&c. At the faster flow rate of 30 ml/min, endothelial cells subjected to ultrasound therapy under a pulsatile flow, with either 0.5 or 1 Hz pulsation frequency, demonstrated a significant enhancement in

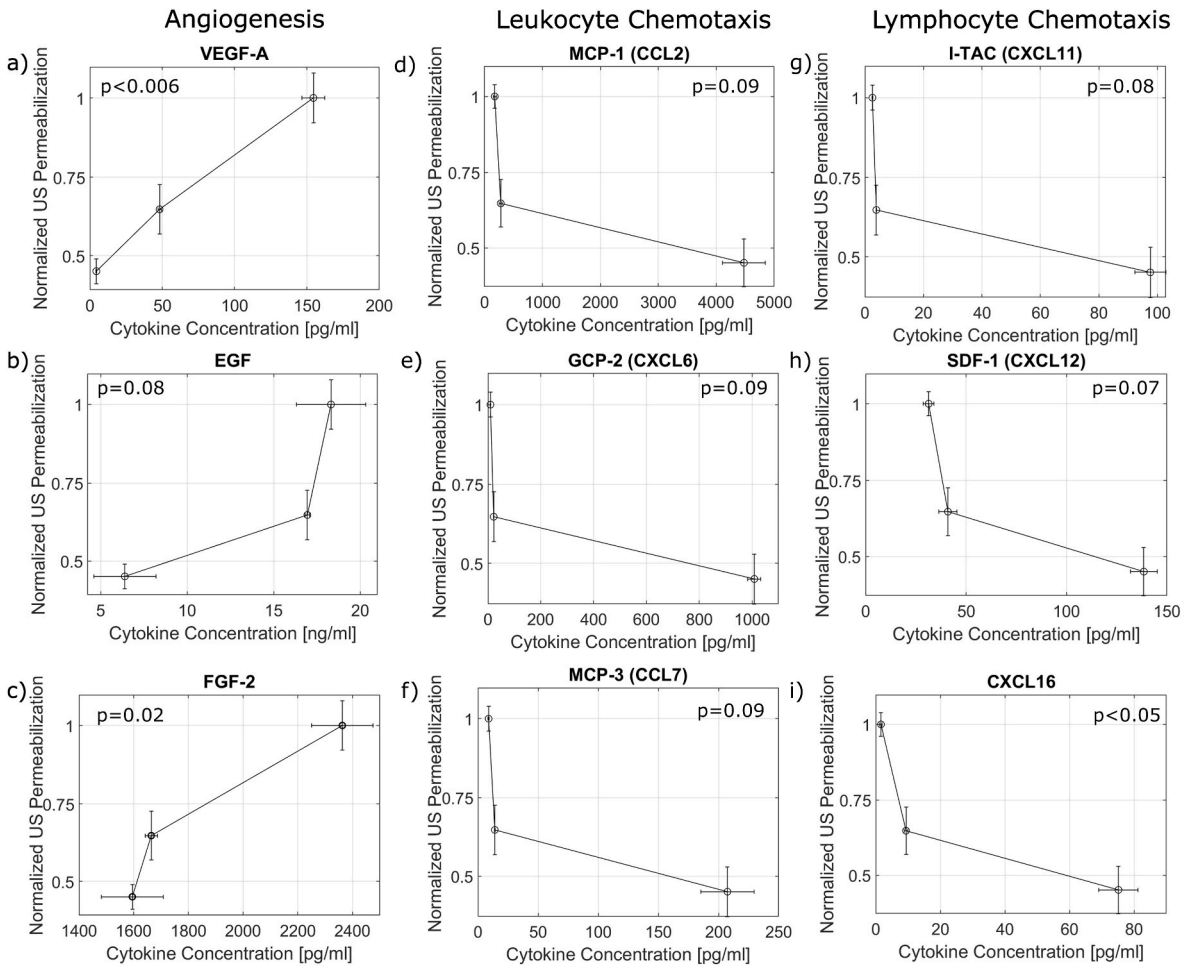

Fig. 4. Microbubble-mediated human endothelial permeability is directly correlated with the presence of pro-angiogenesis markers and inversely correlated with pro-inflammatory ones. a-c) This first column highlights the general positive correlation of VEGF-A, EGF, and FGF-2 and ultrasound treatment – three cytokines with well established roles in angiogenesis. All other analytes show an inverse correlation, including those involved in d-f) leukocyte (MCP-1, GCP-2, MCP-3) and g-i) lymphocyte (I-TAC, SDF-1, CXCL16) chemotaxis. Pearson correlation coefficients range from $0.82 \leq |R| \leq 0.99$, and statistical significance is shown within the panel for each analyte. It is important to note here that many of these are trending towards significance, including others not shown here (*e.g.* IL6). The ultrasound permeabilization quantity shown is normalized to its maximum, taken from the data obtained when treated at 8 dyne/cm^2. This data is strongly suggestive that the local cytokine environment in which the endothelial cells are situated modifies its susceptibility to external perforation.

membrane permeability as compared to those treated under laminar flow by 1.62-fold ($p < 0.05$) and 2.05-fold ($p < 0.001$), respectively. We further confirmed this trend by examining the differential permeability between these two treatment flow patterns at a slower flow rate of 15 ml/min (Fig. 5c). Pulsatile flow with 1 Hz pulsing frequency similarly enhances the extent of cell permeability compared to a flow-matched laminar condition (1.69-fold, $p < 0.001$), however when the interval of time was increased (0.5 Hz) at the slower flow rate, we failed to see an elevated percentage of endothelial cell perforation. We next examined the more complex scenario of microbubble perfusion under reversing oscillatory flow, shown in Fig. 6, under two physiological shear-rates (± 2 dyne/cm^2 and ± 4 dyne/cm^2). First, we examined this effect at a relatively slow flow rate of ± 8 ml/min (3.33 cm/s), in which, independent of oscillation frequency, there was no observable cell permeabilization. When increasing the flow rate to ± 16 ml/min, oscillatory flow at 0.5 Hz increased the percentage of permeabilized cells by 1.76-fold ($p < 0.005$). While reversing oscillatory flow at 1 Hz at this flow rate yielded no significant change as compared to laminar flow, it still indeed induced permeation (unlike at the slower flow rate). To place the results of the effect of microbubble perfusion pattern on ultrasound-assisted membrane permeabilization into context, it is perhaps instructive here to first consider the purely physical argument of local microbubble density and proximity to the endothelial layer. In first considering the non-reversing pulsatile data (Fig. 5), the flow rate of 30 ml/min corresponds to a linear velocity of 12.5 cm/s, given the cross-sectional area of the flow chamber. At this velocity, the microbubbles travel the length of the projected acoustic focus (3.5 mm) in 2.8 ms, with a microbubble displacement of 1.25 mm during the 1 ms PRI (~3 ultrasound bursts per microbubble in principle). During the intervals in which flow is temporarily stopped, the microbubble population will tend towards size stratification via differential flotation [60]. Relatively speaking, these intervals are rather large (1000 ms and 500 ms for 0.5 and 1 Hz pulsing frequency, respectively) compared to the ultrasound PRI, and represent a significant percentage of the treatment duration – fixed to 4 s in this study. In this arrangement and within a fixed time period, the bubble size distribution within close proximity to the endothelial layer slightly shifts to smaller bubbles. Estimation of this differential flotation away from the endothelial monolayer by Stoke's equation yields a ~0.5–35 μm shift for bubbles ranging in radius from $0.5 \leq r \leq 4$ μm within 1 s of flow cessation (0.5 Hz), for example. While this translation may not represent a significant change within the acoustic focus ($\ll 1$ %), it does bring the microbubbles within closer proximity to each other. Indeed, at the bubble dilution used here, the average inter-bubble spacing is ~25 μm. With a net displacement on the order of tens of microns (*i.e.* very small inter-bubble spacings), we can expect to see significant vibrational effects due to the influence of one microbubble on another [61]. Further,

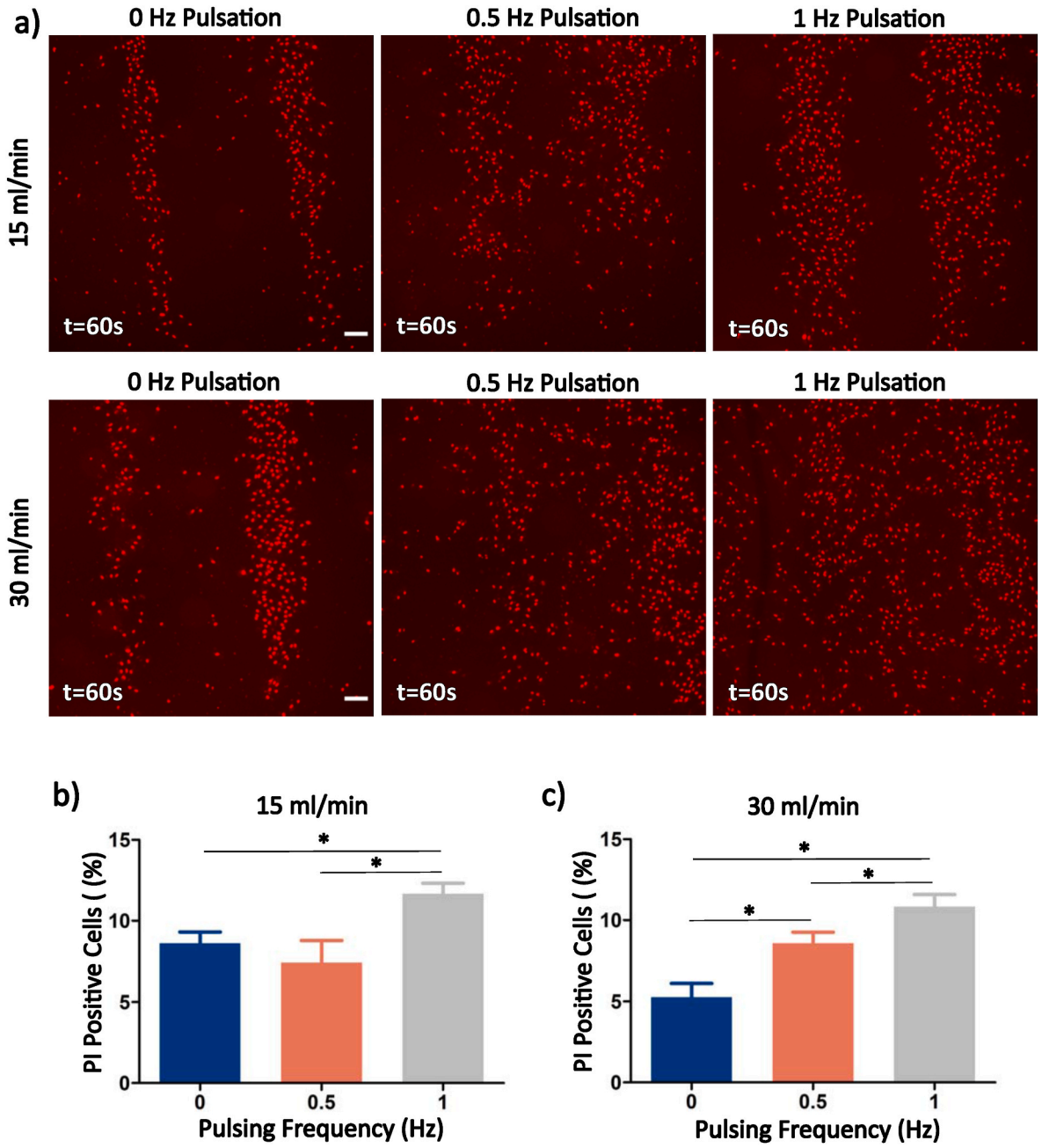

Fig. 5. Pulsatile perfusion of microbubbles influences ultrasound-mediated endothelial cell permeabilization. a) Representative fluorescence images at the end of recording (60 s), illustrating macromolecular uptake under varying flow profiles. Data shown for microbubbles perfusing at 15 ml/min (top panel; ~4 dyne/cm^2) and 30 ml/min (bottom pane, ~8 dyne/cm^2). The scale bar is 50 μm. b) The extent of microbubble-mediated cell perforation significantly increases when perfused at 15 ml/min at 1 Hz pulsation frequency (1.69-fold, $p < 0.001$), while increasing the flow rate to 30/min elevated cell perforation as compared to laminar flow at 0.5 Hz and 1 Hz respectively (1.9-fold, $p < 0.05$; 2.4-fold, $p < 0.001$). These observations underscore the significant influence of microbubble flow dynamics on ultrasound-mediated cell perforation efficacy. Note that laminar flow here is indicated by a pulsing frequency of 0 Hz. Please note that no shear preconditioning was applied here (cells were cultured statically).

the probability of microbubble-microbubble interactions via secondary radiation forces, for example the coalescence of two or more bubbles into a larger bubble, is increased at these shorter inter-bubble distances. It is also important to consider microbubble residence time within the acoustic beam (*e.g.* for the bubbles arrested within the beam for 1 s, the same/similar population will be interrogated 1000 times at this PRI). This represents a trade-off between the propensity of eliciting sufficient microbubble vibration to include membrane permeabilization [19] versus the likelihood for microbubble disruption (and therefore no more sources of localized stresses to permeate cells), both of which increase with number of transmit bursts. At some point during the acoustic pulse, it is indeed probable that microbubble disruption occurs and thus bubble replenishment by the resuming of flow will contribute positively to the number of endothelial cells undergoing ultrasound-assisted permeabilization.

The interactions between the microbubbles circulating under reversing oscillatory flow and the endothelial layer were more heterogeneous (Fig. 6). Circulation of microbubbles flowing at the slower speed (±8 ml/min) corresponds to a linear travel distance of 33.3 μm within the 1 ms PRI, which is approximately the length of the two endothelial cells. In principle, at this slow of a rate, the microbubbles that are entering the acoustic beam are likely undergoing acoustically

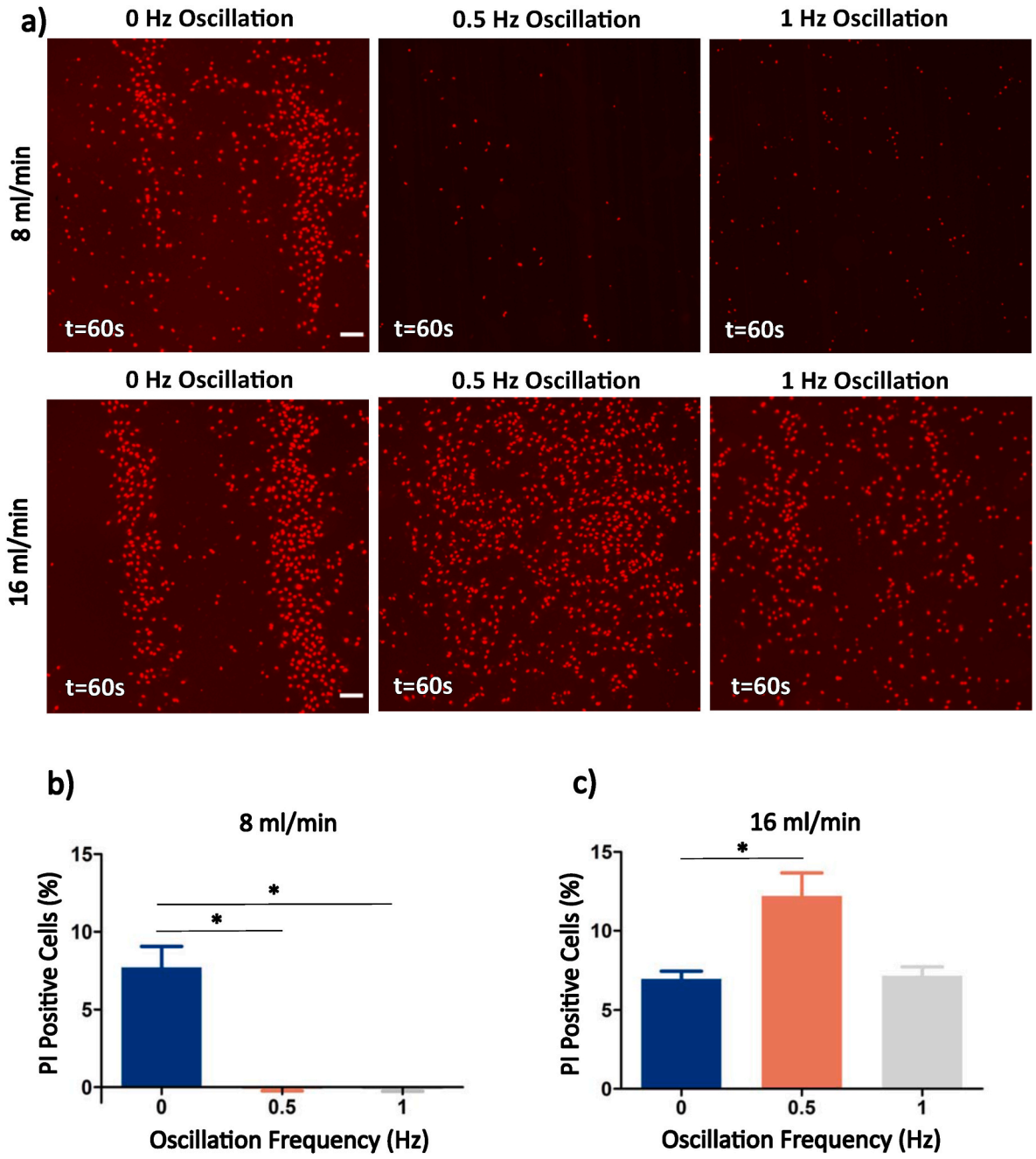

Fig. 6. Oscillatory flow perfusion enhances ultrasound-mediated cell permeabilization when characterized with high flow velocity and low oscillation frequency. a) Representative fluorescence microscopy examples illustrating microbubble-induced cell perforation – indicated here by the presence of an otherwise impermeable macromolecular in red - under varied flow conditions with shear flows of either 8 ml/min (top; ±2 dyne/cm^2) or 16 ml/min (bottom; ±4 dyne/cm^2). Scale bar is 50 μm. Statically cultured cells were perfused with microbubbles under three flow profiles: i) laminar (blue bars), and oscillatory with oscillation frequency of 0.5 Hz (orange bars) or1 Hz (grey bars) and fluid velocity of either b) 8 or c) 16 ml/min. Our results demonstrate a significant enhancement in cell permeability when microbubbles flow at 16 ml/min at 0.5 Hz frequency (1.76-fold, $p < 0.005$), whereas 1 Hz oscillation frequency fails to elevate cell perforation. Interestingly, when perfused at the slower speed of 8 ml/min, a complete suppression of cell permeabilization was observed for either oscillation frequency condition. Note that laminar flow here is indicated by an oscillation frequency of 0 Hz. Please note that no shear preconditioning was applied here (cells were cultured statically).

induced disruption (subjected to ~105 ultrasound bursts while within the acoustic focus). Thus, even within the first positive phase of oscillatory motion, there would be no more microbubbles able to re-enter the acoustic beam – either distally (reverse phase of fluid motion) nor proximally (forward phase) to the acoustic focal zone. At the faster flow rate of 16 ml/min (6.66 cm/s), our hypothesis here is that only partial disruption occurred and thus enables the replenishment of new microbubbles within the acoustic focus. It is important to note here that, even at the slowest microbubble flow rates employed, the imaging frame rate used here (~50 Hz) is too slow to obtain reliable information on microbubble population pattern and acoustically induced disruption. Simultaneous bright-field imaging with a fast-frame camera, with frame rates on the order of kHz, would be an invaluable tool to shed mechanistic insight into the relationship between microbubble translational dynamics and endothelial permeabilization under flow, and is the subject of future endeavors.

4. Conclusion

The effects of fluid flow and the resulting shear stress on microbubble-mediated endothelial cell permeabilization was investigated in two contexts. First, sustained shear-stress preconditioning of human endothelial cells increases their susceptibility to ultrasound-assisted cell membrane permeabilization under identical acoustic stimulation up to 2-fold as compared to non-preconditioned cells. Multiplex examination of the endothelial secretome under these conditions revealed correlations between enhanced ultrasound-assisted cell membrane permeability and expression of cytokines involved in angiogenesis (*e.g.* VEGF-A, EGF, FGF-2) and inflammation – including both leukocyte (*e.g.* MCP-1) and lymphocyte (*e.g.* SDF-1) chemotaxis. Secondly, the microbubble fluid flow pattern (non-reversing pulsatile, reversing oscillatory) as it perfuses endothelial cells significantly modifies the efficiency of this treatment technique given the same acoustic stimulus, resulting in up to a 2.4-fold increase in the percentage of permeability when treated under pulsatile conditions versus a flow rate-matched laminar flow, depending on the specific flow parameters. Reversing oscillatory fluid flow, as compared to laminar flow, can result in up to a 1.7-fold increase or a complete shutdown for endothelial membrane permeability, highlighting a more heterogeneous response. The results from both of these contexts emphasizes the fact that microbubble-assisted therapeutics is strongly dependent on both the pathophysiology of the vascular compartment and the local microbubble density and distribution as it perfuses the vasculature. Among others, this work has implications for emerging anti-inflammatory drug delivery approaches for atherosclerosis, which have had recent success in clinical trials, whereby local conditions of ischemia and disrupted flow with varying magnitudes of shear stress and perfusion pattern are to be expected.

CRediT authorship contribution statement

Elahe Memari: Writing – original draft, Methodology, Investigation, Formal analysis, Data curation. **Brandon Helfield:** Writing – review & editing, Writing – original draft, Visualization, Validation, Software, Resources, Methodology, Investigation, Funding acquisition, Formal analysis, Data curation, Conceptualization.

Declaration of competing interest

The authors declare that they have no known competing financial interests or personal relationships that could have appeared to influence the work reported in this paper.

Data availability

Data will be made available on request.

Acknowledgements

This work was funded by the Canada Research Chairs program (CRC-2023-00137), the Canadian Cardiovascular Society (CCS; 1512960) and the Canadian Institutes of Health Research (CIHR; PJT-190209). Dr. Helfield is a Burroughs Wellcome Fund fellow (1018212.03).

References

[1] G.K. Hansson, P. Libby, The immune response in atherosclerosis: a double-edged sword, Nat. Rev. Immunol. 6 (2006) 508–519, https://doi.org/10.1038/nri1882.
[2] W. Herrington, B. Lacey, P. Sherliker, J. Armitage, S. Lewington, Epidemiology of atherosclerosis and the potential to reduce the global burden of atherothrombotic disease, Circ. Res. 118 (2016) 535–546, https://doi.org/10.1161/CIRCRESAHA.115.307611.
[3] P.F. Davies, Hemodynamic shear stress and the endothelium in cardiovascular pathophysiology, Nat. Clin. Pract. Cardiovasc. Med. 6 (2009) 16–26, https://doi.org/10.1038/ncpcardio1397.
[4] V. Raygor, A. Khera, New recommendations and revised concepts in recent guidelines on the management of dyslipidemias to prevent cardiovascular disease: the 2018 ACC/AHA and 2019 ESC/EAS guidelines, Curr. Cardiol. Rep. 22 (2020), https://doi.org/10.1007/s11886-020-01331-z.
[5] M. Bäck, G.K. Hansson, Anti-inflammatory therapies for atherosclerosis, Nat. Rev. Cardiol. 12 (2015) 199–211, https://doi.org/10.1038/nrcardio.2015.5.
[6] P.M. Ridker, B.M. Everett, A. Pradhan, J.G. MacFadyen, D.H. Solomon, E. Zaharris, V. Mam, A. Hasan, Y. Rosenberg, E. Iturriaga, M. Gupta, M. Tsigoulis, S. Verma, M. Clearfield, P. Libby, S.Z. Goldhaber, R. Seagle, C. Ofori, M. Saklayen, S. Butman, N. Singh, M. Le May, O. Bertrand, J. Johnston, N.P. Paynter, R.J. Glynn, Low-dose methotrexate for the prevention of atherosclerotic events, N. Engl. J. Med. 380 (2019) 752–762, https://doi.org/10.1056/nejmoa1809798.
[7] J.-C. Tardif, S. Kouz, D.D. Waters, O.F. Bertrand, R. Diaz, A.P. Maggioni, F.J. Pinto, R. Ibrahim, H. Gamra, G.S. Kiwan, C. Berry, J. López-Sendón, P. Ostadal, W. Koenig, D. Angoulvant, J.C. Grégoire, M.-A. Lavoie, M.-P. Dubé, D. Rhainds, M. Provencher, L. Blondeau, A. Orfanos, P.L. L'Allier, M.-C. Guertin, F. Roubille, Efficacy and safety of low-dose colchicine after myocardial infarction, N. Engl. J. Med. 381 (2019) 2497–2505, https://doi.org/10.1056/nejmoa1912388.
[8] P.M. Ridker, B.M. Everett, T. Thuren, J.G. MacFadyen, W.H. Chang, C. Ballantyne, F. Fonseca, J. Nicolau, W. Koenig, S.D. Anker, J.J.P. Kastelein, J.H. Cornel, P. Pais, D. Pella, J. Genest, R. Cifkova, A. Lorenzatti, T. Forster, Z. Kobalava, L. Vida-Simiti, M. Flather, H. Shimokawa, H. Ogawa, M. Dellborg, P.R.F. Rossi, R.P.T. Troquay, P. Libby, R.J. Glynn, Antiinflammatory therapy with canakinumab for atherosclerotic disease, N. Engl. J. Med. 377 (2017) 1119–1131, https://doi.org/10.1056/nejmoa1707914.
[9] P.F. Davies, Flow-mediated mechanotransduction, Physiol. Rev. 75 (1995) 519–560.
[10] J.-J. Chiu, S. Chien, Effects of disturbed flow on vascular endothelium: pathophysiological basis and clinical perspectives, Physiol. Rev. 91 (2011) 327–387, https://doi.org/10.1152/physrev.00047.2009.-Vascular.
[11] I.A. Tamargo, K.I. Baek, Y. Kim, C. Park, H. Jo, Flow-induced reprogramming of endothelial cells in atherosclerosis, Nat. Rev. Cardiol. 20 (2023) 738–753, https://doi.org/10.1038/s41569-023-00883-1.
[12] H. Yusefi, B. Helfield, Ultrasound contrast imaging: fundamentals and emerging technology, Front Phys 10 (2022), https://doi.org/10.3389/fphy.2022.791145.
[13] B. Helfield, A review of phospholipid encapsulated ultrasound contrast agent microbubble physics, Ultrasound Med. Biol. 45 (2019) 282–300, https://doi.org/10.1016/j.ultrasmedbio.2018.09.020.
[14] D.E. Goertz, An overview of the influence of therapeutic ultrasound exposures on the vasculature: high intensity ultrasound and microbubble-mediated bioeffects, Int. J. Hyperther. 31 (2015) 134–144, https://doi.org/10.3109/02656736.2015.1009179.
[15] K. Hynynen, N. Mcdannold, N. Vykhodtseva, F.A. Jolesz, Noninvasive MR imaging–guided focal opening of the blood-brain barrier in rabbits, Radiology 220 (2001) 640–646.
[16] Y. Meng, K. Hynynen, N. Lipsman, Applications of focused ultrasound in the brain: from thermoablation to drug delivery, Nat. Rev. Neurol. 17 (2021) 7–22, https://doi.org/10.1038/s41582-020-00418-z.
[17] E. Memari, D. Khan, R. Alkins, B. Helfield, Focused ultrasound-assisted delivery of immunomodulating agents in brain cancer, J. Contr. Release 367 (2024) 283–299, https://doi.org/10.1016/j.jconrel.2024.01.034.
[18] Y. Hu, J.M.F. Wan, A.C.H. Yu, Membrane perforation and recovery dynamics in microbubble-mediated sonoporation, Ultrasound Med. Biol. 39 (2013) 2393–2405, https://doi.org/10.1016/j.ultrasmedbio.2013.08.003.
[19] B. Helfield, X. Chen, S.C. Watkins, F.S. Villanueva, Biophysical insight into mechanisms of sonoporation, Proc. Natl. Acad. Sci. U. S. A. 113 (2016) 9983–9988, https://doi.org/10.1073/pnas.1606915113.
[20] B. Helfield, X. Chen, S.C. Watkins, F.S. Villanueva, Transendothelial perforations and the sphere of influence of single-site sonoporation, Ultrasound Med. Biol. 46 (2020) 1686–1697, https://doi.org/10.1016/j.ultrasmedbio.2020.02.017.
[21] I. Beekers, F. Mastik, R. Beurskens, P.Y. Tang, M. Vegter, A.F.W. van der Steen, N. de Jong, M.D. Verweij, K. Kooiman, High-resolution imaging of intracellular calcium fluctuations caused by oscillating microbubbles, Ultrasound Med. Biol. 46 (2020) 2017–2029, https://doi.org/10.1016/j.ultrasmedbio.2020.03.029.
[22] Z. Fan, R.E. Kumon, J. Park, C.X. Deng, Intracellular delivery and calcium transients generated in sonoporation facilitated by microbubbles, J. Contr. Release 142 (2010) 31–39, https://doi.org/10.1016/j.jconrel.2009.09.031.
[23] J.T. Belcik, B.P. Davidson, A. Xie, M.D. Wu, M. Yadava, Y. Qi, S. Liang, C.R. Chon, A.Y. Ammi, J. Field, L. Harmann, W.M. Chilian, J. Linden, J.R. Lindner, Augmentation of muscle blood flow by ultrasound cavitation is mediated by ATP and purinergic signaling, Circulation 135 (2017) 1240–1252.
[24] F. Moccetti, T. Belcik, Y. Latifi, A. Xie, K. Ozawa, E. Brown, B.P. Davidson, W. Packwood, A. Ammi, S. Huke, J.R. Lindner, Flow augmentation in the myocardium by ultrasound cavitation of microbubbles: role of shear-mediated purinergic signaling, J. Am. Soc. Echocardiogr. 33 (2020) 1023–1031.e2, https://doi.org/10.1016/j.echo.2020.03.016.
[25] D. McMahon, A. Lassus, E. Gaud, V. Jeannot, K. Hynynen, Microbubble formulation influences inflammatory response to focused ultrasound exposure in the brain, Sci. Rep. 10 (2020), https://doi.org/10.1038/s41598-020-78657-9.
[26] E. Memari, F. Hui, H. Yusefi, B. Helfield, Fluid flow influences ultrasound-assisted endothelial membrane permeabilization and calcium flux, J. Contr. Release 358 (2023) 333–344, https://doi.org/10.1016/j.jconrel.2023.05.004.
[27] A. van Wamel, K. Kooiman, M. Harteveld, M. Emmer, F.J. ten Cate, M. Versluis, N. de Jong, Vibrating microbubbles poking individual cells: drug transfer into cells via sonoporation, J. Contr. Release 112 (2006) 149–155, https://doi.org/10.1016/j.jconrel.2006.02.007.

[28] H.Y. Stevens, B. Melchior, K.S. Bell, Y. Sujin, J.C. Yeh, J.A. Frangos, PECAM-1 is a critical mediator of atherosclerosis, DMM Disease Models and Mechanisms 1 (2008) 175–181, https://doi.org/10.1242/dmm.000547.
[29] Z. Chen, E. Tzima, PECAM-1 is necessary for flow-induced vascular remodeling, Arterioscler. Thromb. Vasc. Biol. 29 (2009) 1067–1073, https://doi.org/10.1161/ATVBAHA.109.186692.
[30] A.M. Malek, S.L. Alper, S. Izumo, Hemodynamic shear stress and its role in atherosclerosis, J. Am. Med. Assoc. 282 (1999) 2035–2042. www.jama.com.
[31] D.N. Ku, D.P. Giddens, C.K. Zarins, S. Glagov, Pulsatile flow and atherosclerosis in the human carotid bifurcation positive correlation between plaque location and low and oscillating shear stress, atherosclerosis, Thrombosis, and, Vascular Biology 5 (1985) 293–305. http://ahajournals.org.
[32] R. Goel, B.R. Schrank, S. Arora, B. Boylan, B. Fleming, H. Miura, P.J. Newman, R. C. Molthen, D.K. Newman, Site-specific effects of PECAM-1 on atherosclerosis in LDL receptor-deficient mice, Arterioscler. Thromb. Vasc. Biol. 28 (2008) 1996–2002, https://doi.org/10.1161/ATVBAHA.108.172270.
[33] J.R. Privratsky, D.K. Newman, P.J. Newman, PECAM-1: conflicts of interest in inflammation, Life Sci. 87 (2010) 69–82, https://doi.org/10.1016/j.lfs.2010.06.001.
[34] J.R. Privratsky, C.M. Paddock, O. Florey, D.K. Newman, W.A. Muller, P. J. Newman, Relative contribution of PECAM-1 adhesion and signaling to the maintenance of vascular integrity, J. Cell Sci. 124 (2011) 1477–1485, https://doi.org/10.1242/jcs.082271.
[35] C. Collins, L.D. Osborne, C. Guilluy, Z. Chen, E.T. O'Brien, J.S. Reader, K. Burridge, R. Superfine, E. Tzima, Haemodynamic and extracellular matrix cues regulate the mechanical phenotype and stiffness of aortic endothelial cells, Nat. Commun. 5 (2014), https://doi.org/10.1038/ncomms4984.
[36] P.J. Butler, G. Norwich, S. Weinbaum, S. Chien, S. Chien, Shear stress induces a time- and position-dependent increase in endothelial cell membrane fluidity, Am. J. Physiol. Cell Physiol. 280 (2001) 962–969. http://www.ajpcell.orgC962.
[37] M.A. Haidekker, N. L'heureux, J.A. Frangos, Fluid shear stress increases membrane fluidity in endothelial cells: a study with DCVJ fluorescence, Am. J. Physiol. Heart Circ. Physiol. 278 (2000) H1401–H1406. http://www.ajpheart.org.
[38] T. Shimanouchi, H. Ishii, N. Yoshimoto, H. Umakoshi, R. Kuboi, Calcein permeation across phosphatidylcholine bilayer membrane: effects of membrane fluidity, liposome size, and immobilization, Colloids Surf. B Biointerfaces 73 (2009) 156–160, https://doi.org/10.1016/j.colsurfb.2009.05.014.
[39] F. Berthiaume, J.A. Frangos, Fluid flow increases membrane permeability to merocyanine 540 in human endothelial cells, Biochim. Biophys. Acta Biomembr. 1191 (1994) 209–218.
[40] T. Nozaki, R. Ogawa, L.B. Feril, G. Kagiya, H. Fuse, T. Kondo, Enhancement of ultrasound-mediated gene transfection by membrane modification, J. Gene Med. 5 (2003) 1046–1055.
[41] Y. Gao, Z.S. Galis, Exploring the role of endothelial cell resilience in cardiovascular Health and disease, Arterioscler. Thromb. Vasc. Biol. 41 (2021) 179–185, https://doi.org/10.1161/ATVBAHA.120.314346.
[42] P. Kong, Z.Y. Cui, X.F. Huang, D.D. Zhang, R.J. Guo, M. Han, Inflammation and atherosclerosis: signaling pathways and therapeutic intervention, Signal Transduct. Targeted Ther. 7 (2022), https://doi.org/10.1038/s41392-022-00955-7.
[43] S. Lee, T.T. Chen, C.L. Barber, M.C. Jordan, J. Murdock, S. Desai, N. Ferrara, A. Nagy, K.P. Roos, M.L. Iruela-Arispe, Autocrine VEGF signaling is required for vascular homeostasis, Cell 130 (2007) 691–703, https://doi.org/10.1016/j.cell.2007.06.054.
[44] S.M. Weis, D.A. Cheresh, Pathophysiological consequences of VEGF-induced vascular permeability, Nature 437 (2005) 497–504, https://doi.org/10.1038/nature03987.
[45] S. Esser, K. Wolburg, H. Wolburg, G. Breier, T. Kurzchalia, W. Risau, Vascular endothelial growth factor induces endothelial fenestrations in vitro. http://www.jcb.org, 1998.
[46] G.W. Roberts, G.E. Palade, Increased microvascular permeability and endothelial fenestration induced by vascular endothelial growth factor, J. Cell Sci. 108 (1995) 2369–2379.
[47] X. Bao, C. Lu, J.A. Frangos, Temporal gradient in shear but not steady shear stress induces PDGF-A and MCP-1 expression in endothelial cells role of NO, NFB, and egr-1. http://www.atvbaha.org, 1999.
[48] Y.-J. Shyy, H.-J. Hsieh, S. Usami, S. Chien, Fluid shear stress induces a biphasic response of human monocyte chemotactic protein 1 gene expression in vascular endothelium. https://www.pnas.org, 1994.
[49] A.R. Brooks, P.I. Lelkes, G.M. Rubanyi, Gene expression profiling of human aortic endothelial cells exposed to disturbed flow and steady laminar flow. https://doi.org/10.1152/physiolgenomics.00075.2001.-Subtrac, 2002.
[50] S. Xu, M. Koroleva, M. Yin, Z.G. Jin, Atheroprotective laminar flow inhibits Hippo pathway effector YAP in endothelial cells, Transl. Res. 176 (2016) 18–28.e2, https://doi.org/10.1016/j.trsl.2016.05.003.
[51] Y.C. Tsai, H.J. Hsieh, F. Liao, C.W. Ni, Y.J. Chao, C.Y. Hsieh, D.L. Wang, Laminar flow attenuates interferon-induced inflammatory responses in endothelial cells, Cardiovasc. Res. 74 (2007) 497–505, https://doi.org/10.1016/j.cardiores.2007.02.030.
[52] S.M. Mccormick, S.G. Eskin, L. V Mcintire, C.L. Teng, C.-M. Lu, C.G. Russell, K.K. Chittur, DNA microarray reveals changes in gene expression of shear stressed human umbilical vein endothelial cells, n.d. www.pnas.orgcgidoi10.1073pnas.171259298.
[53] N. Resnick, H. Yahav, A. Shay-Salit, M. Shushy, S. Schubert, L. Chen, M. Zilberman, E. Wofovitz, Fluid Shear Stress and the Vascular Endothelium: for Better and for Worse, 2003.
[54] X. Yu, R. Zhao, S. Lin, X. Bai, L. Zhang, S. Yuan, L. Sun, CXCL16 induces angiogenesis in autocrine signaling pathway involving hypoxia-inducible factor 1α in human umbilical vein endothelial cells, Oncol. Rep. 35 (2016) 1557–1565, https://doi.org/10.3892/or.2015.4520.
[55] M. Werle, U. Schmal, K. Hanna, J. Kreuzer innere, M CP-1 induces activation of MAP-kinases ERK, JNK and p38 MAPK in human endothelial cells. www.elsevier.com/locate/cardiores, 2002.
[56] K. Yamamoto, Y. Nogimori, H. Imamura, J. Ando, Shear stress activates mitochondrial oxidative phosphorylation by reducing plasma membrane cholesterol in vascular endothelial cells, Proc. Natl. Acad. Sci. USA 117 (2020) 33660–33667, https://doi.org/10.1073/pnas.2014029117/-/DCSupplemental.
[57] W. Chen, D.B. Jump, W.J. Esselman, J.V. Busik, Inhibition of cytokine signaling in human retinal endothelial cells through modification of caveolae/lipid rafts by docosahexaenoic acid, Invest. Ophthalmol. Vis. Sci. 48 (2007) 18–26, https://doi.org/10.1167/iovs.06-0619.
[58] G. Meng, Y. Liu, C. Lou, H. Yang, Emodin suppresses lipopolysaccharide-induced pro-inflammatory responses and NF-κB activation by disrupting lipid rafts in CD14-negative endothelial cells, Br. J. Pharmacol. 161 (2010) 1628–1644, https://doi.org/10.1111/j.1476-5381.2010.00993.x.
[59] P. Varshney, V. Yadav, N. Saini, Lipid rafts in immune signalling: current progress and future perspective, Immunology 149 (2016) 13–24, https://doi.org/10.1111/imm.12617.
[60] D.E. Goertz, N. de Jong, A.F.W. van der Steen, Attenuation and size distribution measurements of Definity™ and manipulated Definity™ populations, Ultrasound Med. Biol. 33 (2007) 1376–1388, https://doi.org/10.1016/j.ultrasmedbio.2007.03.009.
[61] H. Yusefi, B. Helfield, The influence of inter-bubble spacing on the resonance response of ultrasound contrast agent microbubbles, Ultrason. Sonochem. 90 (2022), https://doi.org/10.1016/j.ultsonch.2022.106191.